Experimental investigation of a mathematical model for traveling wave ultrasonic motors

M.T. EL HAGRY, A. A. MAHFOUZ, H. S. AHMED
Power Electronic Department
Electronic Research Institute
El Tahrir Str.-Dokki , Cairo, Egypt
EGYPT

Abstract: Ultrasonic motors have many excellent performance features such as high-holding torque, high driving torque at low speed, silent operation, compactness, and no electromagnetic interferences. Due to such characteristics these motors have a potential for many applications such as automation, and robotics. The performance estimation of the ultrasonic motor is a function of operating conditions such as stiffness, number of piezoelectric segments, motor diameter, etc. Such performance is modeled using the accurate parameters of the motor. In this paper, the derivation of a mathematical model for traveling wave ultrasonic motors and its experimental validation is presented. The different components of the motor have been modeled individually. The resulting submodels are then assembled together to give the model of the complete motor. In order to validate the model, it is simulated with properly parameters and compared with experimental results obtained from an actual traveling wave ultrasonic motor "Shinsei USR60". Good agreement is obtained between simulated and experimental results.

Key-Words: Piezoelectric effect, Ultrasonic motors, Piezomotor, Matahmetical model, Equivalent Circuit

1. Introduction

Recently, ultrasonic motors (USMs) have attracted considerable attention as a new type of actuator in servo-systems. They have many features such as high driving torque at low rotational speed, high holding torque without applied electric power, extremely low noise in operation, simple mechanical design and fast response. There are many types of the ultrasonic motor such as inchworm, inertial stepping, traveling wave, standing wave, mode conversion, and multi-mode conversion motors. Traveling wave ultrasonic motor (TWUM) is considered the most popular types of ultrasonic motors because of its improved efficiency, and life cycle over the other types.

Ultrasonic motors are piezoelectric-based motors. The principle of operation of such a type of motors is based on the utilizing the reverse piezoelectric effect for converting electrical power into mechanical vibrations. The conversion from electrical to mechanical energy of these motor takes place in two stages. The first stage deals with converting the electrical power into a high frequency mechanical vibration to induce traveling or standing waves at the stator surface with frequencies in the ultrasonic range, this is called as electromechanical energy conversion. The second stage deals with converting such mechanical vibration into a frictional force between the rotor and the stator which causes the rotor to move, this is called the mechanical energy conversion.

During the last decade, the efforts of many researchers have been directed towards developing valid models of ultrasonic motors. Due to the popularity of the rotary traveling wave ultrasonic motors and their various applications, most of the developed models were concerned with such a type of ultrasonic motors. There are three approaches, namely: The Equivalent Circuit, the Finite Element, and the mathematical "mechanical". The Equivalent Circuit model is simpler than two models but such technique can not be give the exact performance characteristics of the ultrasonic motor because some parameters are neglected. Also, the finite element

model is much more complicated and time consuming. Several motors have been simulated using this method[5], however the results were not satisfactory because the given models is not the complete one. In this paper the mathematical model of the traveling wave ultrasonic motor is derived in details. Mathematical description of all components of the model was represented in Matlab-Simulink simulation environment. Also, the experimental results are presented and compared to the results of the simulation.

2. Basic Operation of TWUM

The rotary TWUM is shown in Fig. 1. Such a motor consists of the stator and the rotor parts. The stator has only one thin piezoelectric ceramic ring adhered to the opposite face of elastic body. Such piezoelectric ring is divided into two halves, namely, sections A and B. Each section consisting of 8-sectors polarized oppositely in the direction of thickness. Each sector corresponds to half wavelength of the bending wave as shown in Fig. 2. The rotor consists of a moving body, bearing, and a pressing spring [1, 2].

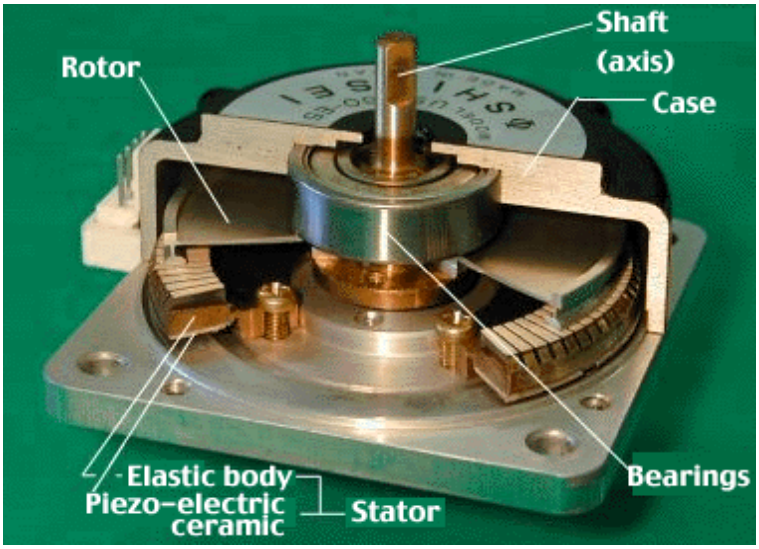

Fig. 1: Cutaway view of the Shinsei USR60 traveling wave ultrasonic motor

When a two phase high frequency sinusoidal voltages with 90^o phase difference are applied to each of the orthogonal halves of the stator, the ceramic sectors of the piezoelectric ring of the stator are expanding and contracting periodically according to the direction of poling. This causes a bending oscillation at the surface of the elastic body, which produces two orthogonal standing waves. The final produced traveling wave is simply the superposition of such a two standing waves. The elliptical motion of the stator surface points is generated by a traveling wave in the stator.

Then the rotor is driven by the tangential force at the stator/rotor contact region resulting from the elliptical motion at each of wave crest. The rotation direction of the rotor is opposite to the direction of the traveling wave propagation [3-5]. The propagation direction of the traveling wave, and thus the rotation direction of the rotor, may be reversed by changing the sign of only one of the driving signals of either piezoelectric half section [6].

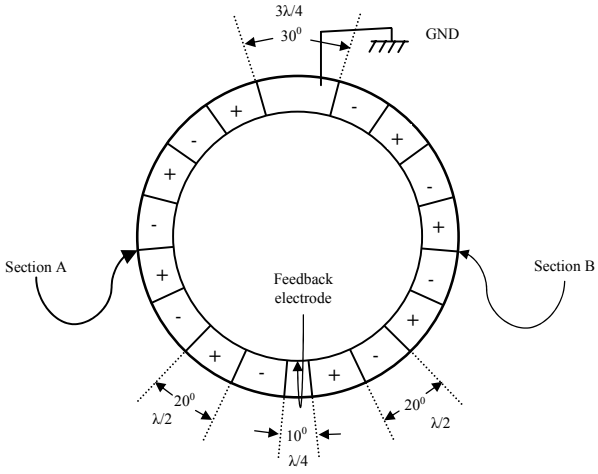

Fig. 2: Piezoelectric ring sectors of the USR60

3. Modeling of the TWUM

The total system for the two-phase rotary TWUM can be divided into its functional modules, as shown in Fig. 3, which are, resonant inverter, piezoelectric thin ring, elastic body, stator/rotor contact, and rotor with load. The complete mathematical model of each functional module of the total system will be derived below.

3.1 Modeling of the Resonant Inverter

The applied voltage to the traveling-wave ultrasonic motor is high frequency sinusoidal waveforms. Fig. 4 shows one phase circuit diagram of a two phase resonant inverter. The main function of resonant inverter is to generate two phase high frequency sinusoidal voltages with the ability to control the amplitude, frequency, and phase shift between them.

The inductor L_s is inserted in a series with piezoelectric ceramic elements for each phase of the inverter.

This is to resonant with the inherent parasitic capacitance C_d of the ultrasonic motor to achieve a sinusoidal wave form and improve the power factor since the ultrasonic motor has capacitive input impedance.

The equivalent circuit of each phase of the resonant inverter is shown in Fig. 5 with the primary side quantities are refered to the secondary side[7-12]. Where inverters MOSFETs losses are equal to 2RDson, the transformer parameters are R_{cu}, L_l, and L_{mg}. The losses in series inductor L_s of the resonant circuit are represented by a series resistance R_{Ls}. So, the values $Rs = R_{cu}+R_{Ls}$, $L_s^{'} = L_l + L_s$, and the primary side parameters become as: $v_{inv}^{'} = n_T v_{inv}$, $i_{inv}^{'} = 1/n_T i_{inv}$, $R_{inv}^{'} = n_T^2 2R_{DSon}$

The output voltage v_{cp} of such a circuit, shown in Fig. 5, is applied to the mechanical part of the ultrasonic motor. The transfer function which describes the previous circuit, Fig. 5, is given by:

$$\frac{v_{cp}}{v_{inv}^{'}} = \frac{k_4.s^3 + k_5.s^2 + k_6.s}{k_4.s^3 + A_4.s^2 + A_5.s + A_6} * \frac{R_d}{k_1.s^2 + k_2.s + k_3} \quad (1)$$

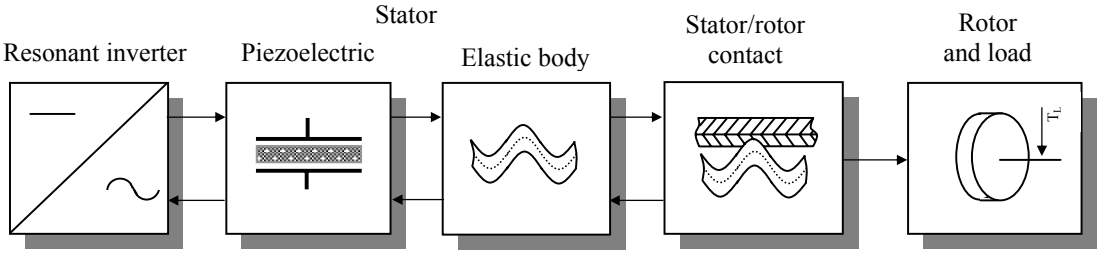

Fig. 3: Block diagram of the total ultrasonic drive system

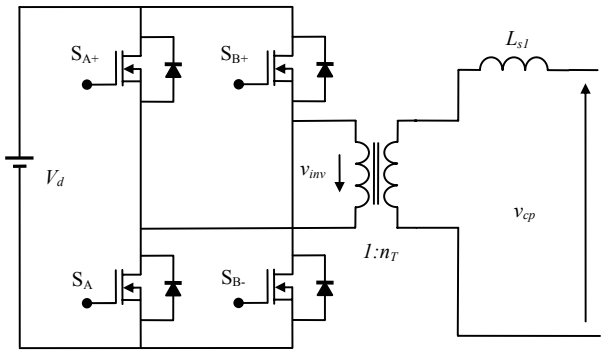

Fig. 4: One phase of resonant inverter

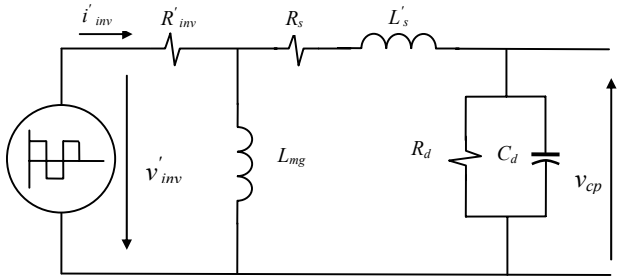

Fig. 5: Model of one of the resonant inverter

3.2 Stator Modeling

The mathematical model of the stator depends on representing the "vibrating piezoelectric ceramic and the elastic body" of the stator by a two mechanical model, namely section A and section B,

as shown in Fig. 6. Such models represent the two sections of the stator and driven by the resonant inverter, that generates sine and cosine voltages v_{cp1} and v_{cp2}, Fig. 2.

The amplitudes of such mechanical vibration modes are $w_{1,t}$ and $w_{2,t}$. The parameter m describes the model mass of the elastic body of stator and ceramic. The parameters d_{s1} and d_{s2} reflect the structural damping of section A and section B respectively.

The parameters C_{s1} and C_{s2} represent the equivalent mechanical stiffness of section A and section B respectively which are the summation the stiffness of the elastic body and stiffness of the piezoelectric ceramic. The cross-couplings between the two modes are represented by symmetry disturbances ε_1, ε_2.The output quantities of the resonant inverter v_{cp1} and v_{cp2} excite the mechanical model of the stator. The parameters A_1 and A_2 represent the electromechanical coupling coefficient.

The motion equations of the mechanical model in Fig. 6 are described as the following state equations [11, 13-15].

Where, the effect of the stator/rotor-contact to the above motion equations is represented by the two nonlinear friction forces F_{d1} and F_{d2}.

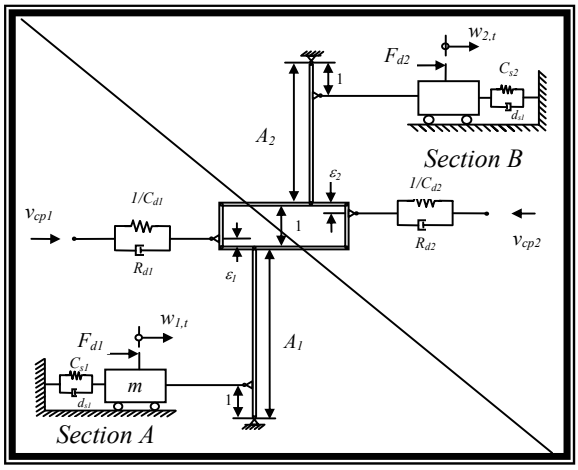

Fig. 6: the two-mode mechanical model of the stator

$$\begin{bmatrix} m & o \\ 0 & m \end{bmatrix}\begin{bmatrix} \ddot{w}_{1,t} \\ \ddot{w}_{2,t} \end{bmatrix}+\begin{bmatrix} d_{s1} & 0 \\ 0 & d_{s2} \end{bmatrix}\begin{bmatrix} \dot{w}_{1,t} \\ \dot{w}_{2,t} \end{bmatrix}+\begin{bmatrix} C_{s1} & 0 \\ 0 & C_{s2} \end{bmatrix}\begin{bmatrix} w_{1,t} \\ w_{2,t} \end{bmatrix}=\begin{bmatrix} A_1(1+\varepsilon_1) & A_1\varepsilon_2 \\ A_2\varepsilon_1 & A_2(1+\varepsilon_2) \end{bmatrix}\begin{bmatrix} v_{cp1} \\ v_{cp2} \end{bmatrix}+\begin{bmatrix} F_{d1} \\ F_{d2} \end{bmatrix} \quad (2)$$

3.3 Stator/Rotor Contact Modeling

Stator-rotor contact model is the most complex part of the whole model of the ultrasonic motor. Stator is assumed to be rigid, which means that the vibration profile is unchanged after the contact with the rotor, whereas rotor has an elastic contact layer.

An unsymmetrical contact mechanism for an arbitrary "wave crest" is depicted in Fig. 7. The stator is assumed to be rigid while the elastic contact layer of the rotor is modeled as a linear spring with equivalent stiffness C_N in axial direction, and rigid in tangential direction [16, 17]. The equivalent stiffness C_N of the contact layer is given by,

$$C_N = Eb / h_r \quad (3)$$

Where:

E: is Young's modulus of the contact layer,

h_r: is the thickness of the contact layer,

b : is the contact width in radial direction.

It is assumed that only two mechanical modes can be excited within the piezoelectric plate. So, two standing waves will be generated. Traveling wave can be generated by superimposing two standing waves. The standing wave equation for the section A and section B can be written as follows

$$w_1(\tilde{x},t) = w_{1,t}.\sin k\tilde{x} \quad (4)$$

$$w_2(\tilde{x},t) = w_{2,t}.\cos k\tilde{x} \quad (5)$$

where,

$$w_{1,t} = \hat{w}_1 \sin \omega t$$

$$w_{2,t} = \hat{w}_2 \cos \omega t_t$$

The equations of the traveling wave and the tangential velocity can be expressed in general form as follows:

$$w(\tilde{x},t) = \sqrt{w_{1,t}^2 + w_{2,t}^2}.\cos(k\tilde{x} - \arctan\frac{w_{1,t}}{w_{2,t}}) \quad (6)$$

$$v_h(\tilde{x},t) = -ak\sqrt{\dot{w}_{1,t}^2 + \dot{w}_{2,t}^2}.\cos(k\tilde{x} + \arctan\frac{\dot{w}_{1,t}}{\dot{w}_{2,t}}) \quad (7)$$

To simplify the above equations (6) and (7), a linear transformation of the original fixed coordinate system may be performed. The new origin x=0 is located at the top of wave crest and moves with same velocity of the traveling wave. The transformation equation between a fixed coordinate system and a moving coordinate system is given as:

$$x = \tilde{x} - \frac{1}{k}\arctan\frac{w_{1,t}}{w_{2,t}} \tag{8}$$

Then, the vertical displacement is therefore

$$w\ (x,t) = \hat{w}(t).\cos(kx) \tag{9}$$

where

$$\hat{w} = \sqrt{w_{1,t}^2 + w_{2,t}^2}$$

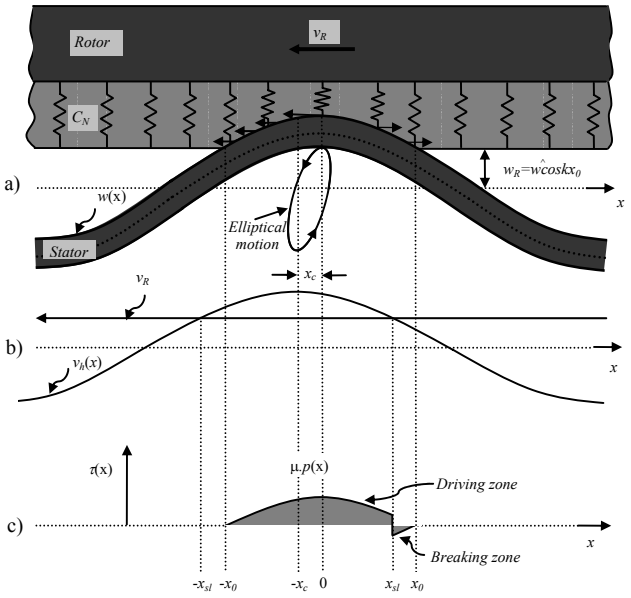

Fig. 7: unsymmetrical contact mechanism.
a) Overlap between stator and elastic contact layer
b) Distribution of stator velocity and rotor velocity
c) Distribution of tangential stresses

Also, The horizontal velocity of the stator surface points becomes as follows:

$$v_h(x,t) = \hat{v}_h(t).\cos(kx + kx_c(\mathrm{t})) \tag{10}$$

where

$$\hat{v}_h = -ak\sqrt{\dot{w}_{1,t}^2 + \dot{w}_{2,t}^2} \tag{11}$$

and

$$kx_c = \arctan\frac{w_{1,t}\,\dot{w}_{1,t} + w_{2,t}\,\dot{w}_{2,t}}{\dot{w}_{2,t}\,w_{1,t} - \dot{w}_{1,t}\,w_{2,t}} \tag{12}$$

Where kx_c is the phase shift between the vertical displacement $w\ (x,t)$ and the stator velocity $v_h(x,t)$. The amplitude $\hat{w}(t)$ of the traveling wave, the maximum of horizontal velocity $\hat{v}_h(t)$, and also the phase shift $kx_c(\mathrm{t})$ are varying with time. It is clear that in such a case the points with maximum horizontal velocity are not in the peaks of the traveling wave as shown in Fig. (7).

For the ideal conditions case, amplitudes of both standing waves are equal and the phase shift between the two modal displacements is 90 degrees. In such a case $\hat{w}$, $\hat{v}_h$ are constants and do not vary with time but kx_c is equal to zero as shown in symmetrical contact mechanism shown in Fig. (8). in this case, the vertical displacement and the horizontal velocity become as follows:

$$w\ (x) = \hat{w}\cos(kx) \tag{13}$$

$$v_h(x) = \hat{v}_h.\cos(kx) \tag{14}$$

From equations (13) and (14), it is clear that the peak of the horizontal velocity occurs at the peak of the vertical displacement because phase shift is equal zero. Also, the points at the peaks of traveling wave move with the highest horizontal velocity.

The overlap Δw between the rotor and the stator is given by,

$$\Delta w = \hat{w}(\cos kx - \cos kx_0) \tag{15}$$

The penetration of stator into the contact layer of the rotor causes the creation of normal contact pressure $p(x)$ along the contact zone. Such a contact pressure is distributed along the contact region $-x_0 \le x \le x_0$ as follows:

$$\begin{aligned} p(x) &= C_N.\Delta w \\ &= C_N.\hat{w}(\cos kx - \cos kx_0) \end{aligned} \tag{16}$$

According to Coulomb's friction law, the tangential stresses $\tau\ (x)$ along the contact region is calculated by

$$\tau(x) = \text{sgn}(|v_h(x)| - |v_R|).\mu.p(x) \quad (17)$$

Where v_R is tangential velocity of the rotor. The tangential stress is in the circumferential direction, but the sign of the tangential stress $\tau(x)$ is related to the velocity v_h of the stator and to the tangential velocity of the rotor v_R at radius ($r=R_w$). The driving force F_R is given by the following equation,

$$F_R = n\mu \int_{-x_0}^{x_0} \text{sgn}(|v_h(x)| - |v_R|).p(x)dx \quad (18)$$

Using the contact pressure $p(x)$ in equation (16) then,

$$F_R = 2n\mu \frac{C_N}{k} \hat{w} \phi_r(x) \quad (19)$$

Where,

$$\phi_r(x) = \sin kx - kx \cos kx_0 \quad (20)$$

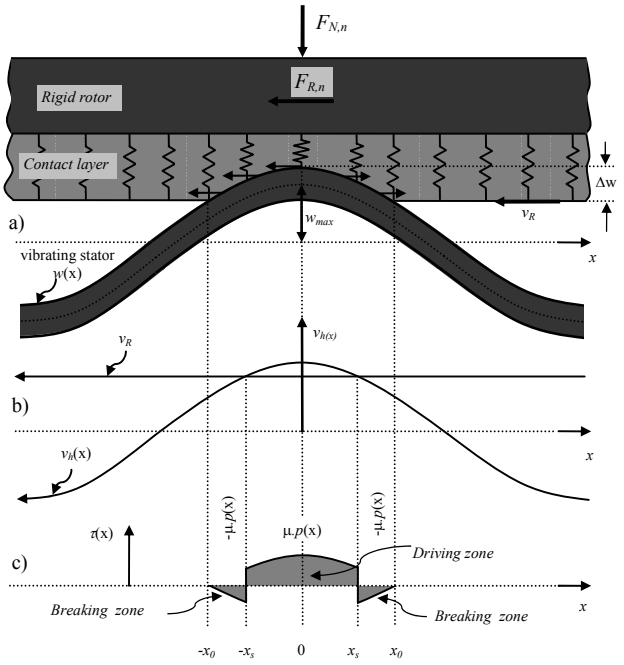

Fig. 8: Ideal Stator/rotor contact mechanism.
a) Overlap between the stator and elastic contact layer
b) Distribution of stator velocity and rotor velocity
c) Distribution of tangential stresses

In order to complete the simulation model of the ultrasonic motor system, the feedback effect of the stator/rotor-contact on the stator's vibration should be included. The contact forces F_{dn} and F_{dt} can be obtained from the effect of the contact pressure $p(x)$ in the normal direction, and the tangential stress in the tangential direction respectively [16, 18]. Then, the equation of F_{dn} and F_{dt} can be written as following,

$$F_{dn} = -n \int_{-x_0}^{x_0} \underset{\sim}{\Phi}_{x}^{T}.p(x)dx \quad (21)$$

$$F_{dt} = n\mu a \int_{-x_0}^{x_0} \frac{\partial \underset{\sim}{\Phi}_{x}^{T}}{\partial \tilde{x}}.\text{sgn}(|v_h(x)| - |v_R|).p(x)dx \quad (22)$$

Where $\underset{\sim}{\Phi}_{x} = \begin{bmatrix} \sin k\tilde{x} & \cos k\tilde{x} \end{bmatrix}$

The final equations of the nonlinear forcing vectors are given by

$$F_{dn} = -n \frac{C_N}{k} \begin{bmatrix} w_{1,t}(kx_o - 1/2 \sin 2kx_o) \\ w_{2,t}(kx_o - 1/2 \sin 2kx_o) \end{bmatrix} \quad (23)$$

$$F_{dt} = n\mu a C_N \begin{bmatrix} w_{1,t}\gamma_e(x) + w_{2,t}\gamma_o(x) \\ w_{2,t}\gamma_e(x) - w_{1,t}\gamma_o(x) \end{bmatrix} \quad (24)$$

Where,

$$\gamma_e(x) = \frac{1}{4}\cos 2kx - \cos kx \cos kx_0$$

$$\gamma_o(x) = \frac{1}{2}kx + \frac{1}{4}\sin 2kx - \cos kx_0 \sin kx$$

The tangential forcing vector and the driving force equations in general form are given as follows:

$$F_R = 2n\mu \frac{C_N}{k} w(\phi_r(x_{sr}) + \phi_r(x_{sl}) - \phi_r(x_o)) \quad (25)$$

$$\begin{aligned} F_{dt1} = -2n\mu a C_N ((&w_{1,t}\gamma_e(x_{sr}) + w_{2,t}\gamma_o(x_{sr})) \\ &- (w_{1,t}\gamma_e(-x_{sl}) + w_{2,t}\gamma_o(-x_{sl})) \\ &- w_{2,t}\gamma_o(x_o)) \end{aligned} \quad (26)$$

$$\begin{aligned} F_{dt2} = -2n\mu a C_N ((&w_{2,t}\gamma_e(x_{sr}) - w_{1,t}\gamma_o(x_{sr})) \\ &- (w_{2,t}\gamma_e(-x_{sl}) - w_{1,t}\gamma_o(-x_{sl})) \\ &+ w_{1,t}\gamma_o(x_o)) \end{aligned} \quad (27)$$

The generated torque T_R of the ultrasonic motor with radius R_w is given as follows:

$$T_R = R_w F_R \quad (28)$$

Where Rw is the radius of the rotor

3.4 Rotor Modeling

The rotor has two degrees of freedom. The first is the rotation of the rotor and the second is the vertical motion in z-direction [19-21]. Fig. (9) shows the mechanical equivalent of the vertical motion of rotor. The dynamic equation of the vertical motion of the rotor is obtained through the force equilibrium in z-direction as follows:

$$m_R \ddot{w}_R + d_Z \dot{w}_R + + c_Z w_R = F_Z - F_N$$

$$= n\int_{-x_0}^{x_0} p(x)dx - F_N = 2n\frac{C_N}{k}\hat{w}\phi_r(x_o) - F_N \quad (29)$$

where

m_R : is the rotor mass,

d_Z : is the equivalent vertical damping

C_z : is the equivalent stiffness,

F_N : is the axial applied force to the rotor by the rotor's disk spring.

The rotational motion equation of the rotor is given by:

$$J\dot{\omega}_R = T_R - T_L \quad (30)$$

The rotor velocity vR is given by:

$$v_R = \omega_R R_w \quad (31)$$

Where

ω_R : is the rotational rotor speed (rad/s),

T_L : is the applied load torque,

J : is the rotor inertia.

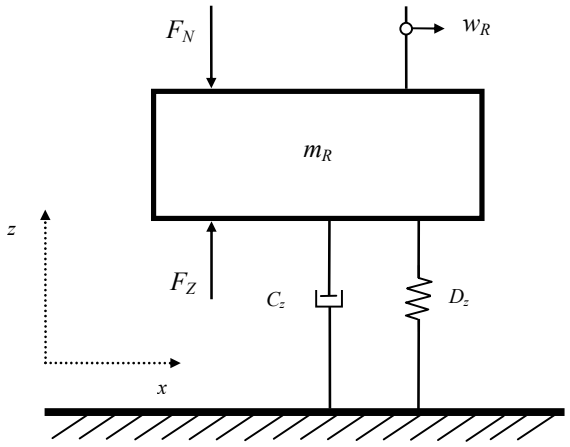

Fig. 9: Mechanical model of the rotor vertical motion

The vertical displacement of the rotor w_R(t) is equal to the vertical stator surface displacement at the edge of the contact region. So, the following equation will be considered to compute the value of x_0:

$$w_R(t) = \hat{w}(t).\cos(kx_0) \quad (32)$$

Then,

$$x_o = \frac{1}{k}\arccos\left|\frac{w_R}{\hat{w}}\right| \quad (33)$$

To calculate the stick points x_{sl} and x_{sr}, at these points, the rotor velocity and horizontal velocity of the stator surface points must be equal. The x_{sl} and x_{sr} equations are given as follows

$$x_{sr} = \frac{1}{k}\arccos\left|\frac{v_R}{\hat{v}_h}\right| - xc \quad (34)$$

$$x_{sl} = \frac{1}{k}\arccos\left|\frac{v_R}{\hat{v}_h}\right| + xc \quad (35)$$

4. Simulation Results

The models explained in the previous subsections are the complete description of the modeling of ultrasonic motor and driver circuit. The equations are simulated using the Matlab and Simulink program. The following simulation results are obtained for the Shinsei USR60 traveling wave ultrasonic motor assuming symmetrical structure ' ideal traveling wave'. The motor parameters used in simulation are taken from motor model USR60 develop commercially by Shinsei and are listed in Appendix A.

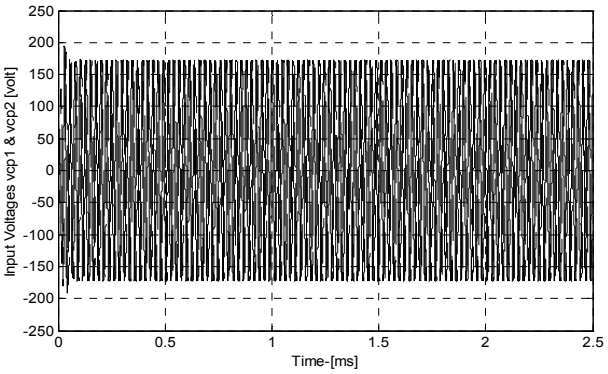

Fig. 10: input voltages v_{cp1} and v_{cp2}

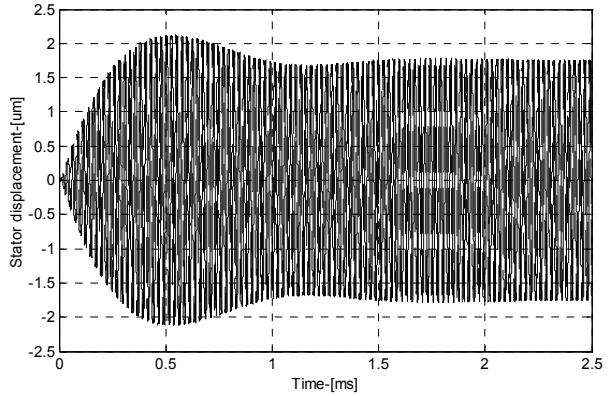

Fig. 11: the stator modal amplitudes $w_{1,t}$ and $w_{2,t}$

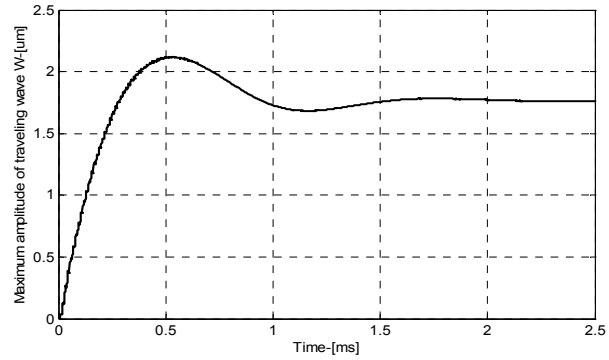

Fig. 12: the amplitude of the traveling wave

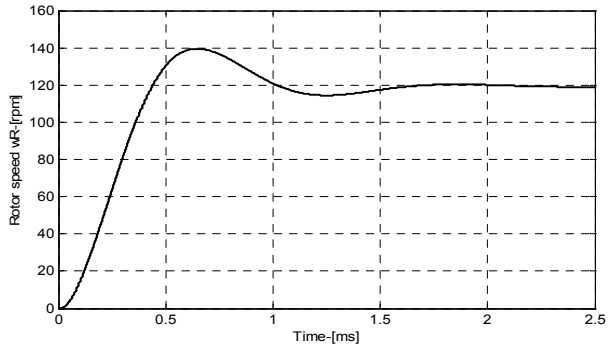

Fig. 13: the rotor speed of ultrasonic motor

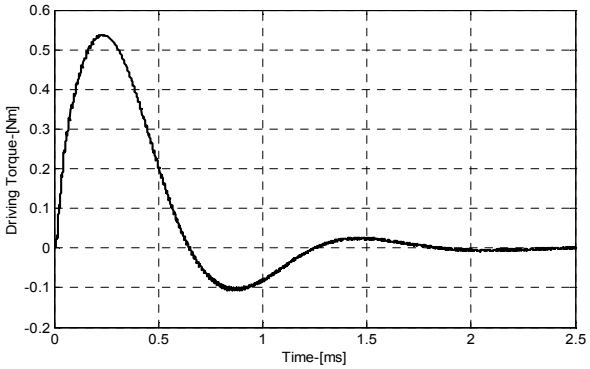

Fig. 14: the generated torque of ultrasonic motor

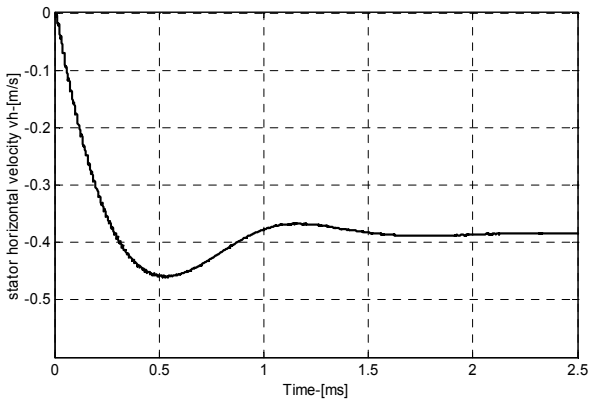

Fig. 15: the stator horizontal velocity v_h

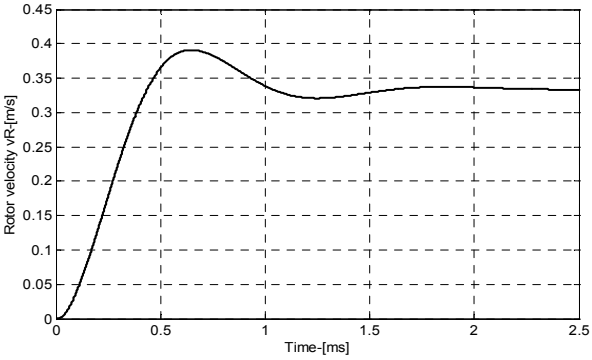

Fig. 16: the stator horizontal velocity v_h

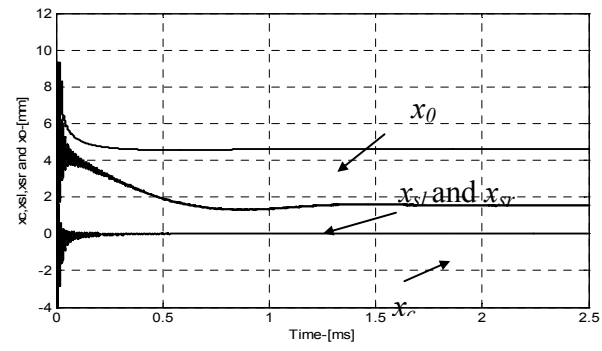

Fig. 17: the stick points x_{sl}, x_{sr}, and point x_0

Fig. 11 shows the stator mechanical amplitudes $w_{1,t}$ and $w_{2,t}$, At the first of the transient time, the mechanical amplitudes $w_{1,t}$ and $w_{2,t}$ of the are still small but the contact zone stretches over the whole wavelength of the traveling wave. As the transient time is increase, the mechanical amplitudes $w_{1,t}$ and $w_{2,t}$ of the stator increase and the contact zone becomes narrower

Also, the motor provide high starting torque, which decreases approaches zero value in the steady state in the case of no load. Torque provided by the stator to the rotor is also shown in Fig. 14. The same phenomenon can also be observed from the Fig. 17 which show the transient response of the no-slip points. At first, position of the no-slip points is far from the wave peak, which means that the driving zone prevails the contact zone. But later on, the no-slip points approach a constant smaller value (i.e. driving zone shrinks), so that driving zone is in balance with braking zones. At the steady state, the torque approaches zero value. The model shows that the motor is characterized by very short transient time (about 1.7ms) which is important advantages of the ultrasonic traveling wave motors. This makes them useful in applications with fast response demands.

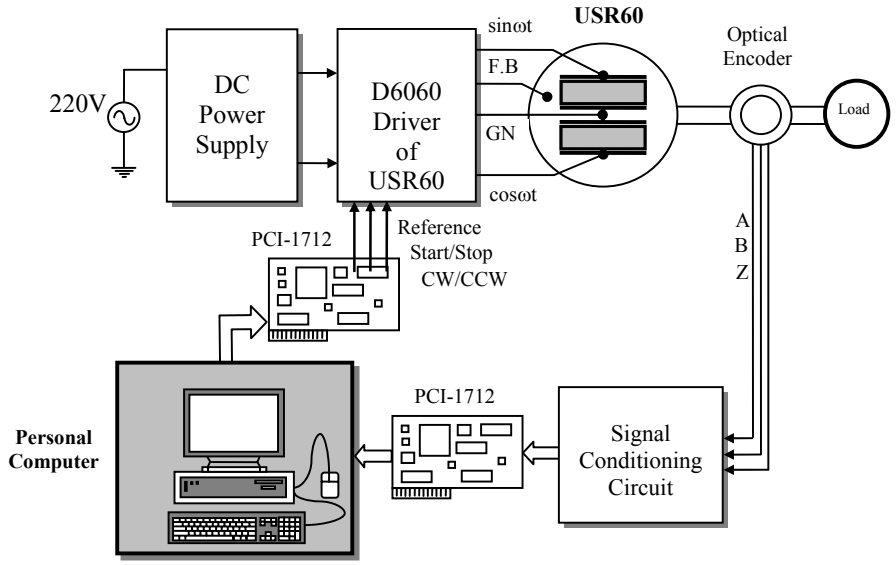

Fig. 18: PC-based Computer Control System for the Shinsei USR60 Drive

5 Experimental Work

Fig. 18 shows the block diagram of the PC-based control for driving the Shinsei USR60 motor. The speed of the motor can be controlling by adjusting the driving frequency f, the phase difference angle ϕ ,and the voltage amplitude of two sinusoidal voltages applied to the motor terminals. The experimental results of the rotary traveling wave are performed in open loop under the effect of the driving frequency and compared with the simulation results. Fig. 19 shows the simulation and experimental response of the speed-frequency characteristic. Such characteristic indicate the similarities between the simulation and experimental result.

6. Conclusions

The complete model of the traveling wave ultrasonic motor is derived in details. The simulation results are compared with the experimental ones which give good agreement of the model. the mathematical model is quite efficient for modeling all parts of the motor. Moreover, such a mathematical model is quit general to handle any type of the traveling wave ultrasonic motors.

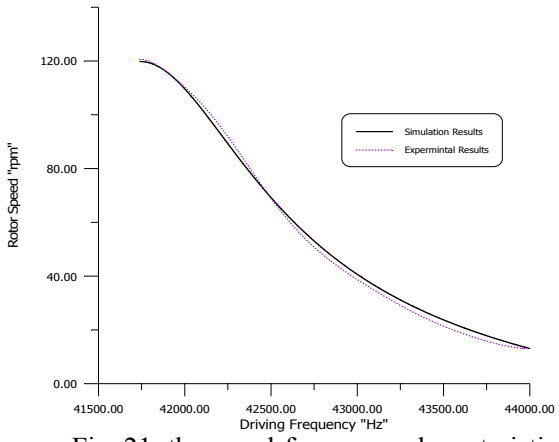

Fig. 21: the speed-frequency characteristic

References

[1] Hagedorn P. and Wallaschek J. "Traveling wave ultrasonic motors: part I. Working principle and mathematical modeling of the stator", Journal of Sound and Vibration, Vol. 155(1), pp31–46,1992

[2] Hagedorn P. and Wallaschek J. "Traveling wave ultrasonic motors: part II. Numerical Method for the flexural vibrations of the stator", Journal of Sound and Vibration, Vol. 168(1), pp115–122,1993

[3] Yoseph Bar-Cohen and Willem Grandia " Rotary Ultrasonic Motors Actuated By Traveling Flexural Waves ", Proceedings of the Smart Structures and Materials Symposium, San Diego, CA, 1998, P3329-82

[4] Xiaoqi Bao and Yoseph Bar-Cohen "Complete Modeling of Rotary Ultrasonic Motors Actuated By Traveling Flexural Waves" Proceedings of SPIE conference, 2000, pp1-7

[5] Takashi Maeno and Akira Miyake "Finite-Element Analysis of the Rotor/Stator Contact in a Ring-type Ultrasonic Motor", IEEE Trans. Ultrasonic, Ferroelectric, and Frequency Control. Vol.39, No.6, 1992, pp.668-674.

[6] Timothy S. Glenn and Nesbitt W. Hagood "Development of a two-sided piezoelectric rotary ultrasonic motors for high torque", Proceedings of SPIE's, Vol. 3041, 1997, pp326-338.

[7] Shin-ichi and Mutsuo Nakaoka "Load-Adaptive frequency tracking control implementation of two–phase resonant inverter for ultrasonic motor", IEEE Trans. Power electronics, Vol.7, No.3, 1992, pp.542-550.

[8] J. Maas, N. Frhleke, P. Krafka, and H. Grotstollen " Prototype Drive and Modulation Concepts for DSP-Controlled Ultrasonic Motors powered by Resonant Converters", Proceedings of EPE'95, Sevilla (Spain), pp. 1777-1782, 1995.

[9] Faa-Jeng and Rou-Yong Duan "Fuzzy neural networks for identification and control of ultrasonic motor drive with LLCC resonant technique," IEEE Trans. Industrial Electronics, Vol. 46, No. 5, 1999, pp 999-1011.

[10] Yuji Izuno, Teruyuki Izumi, Hidenobu Yasutsune, Eiji Hiraki, and Mutsuo Nakaoka "Speed Tracking Servo Control System Incorporating Traveling-Wave-Type Ultrasonic Motor and Feasible Evaluations" IEEE Trans. Industry Applications, Vol. 34, No. 1,1998,pp126-132.

[11] Krome J. W., Maas J, and Wallaschek J "Models for the electro-mechanical interaction of the stator of a piezoelectric ultrasonic motor and its power supply" Journal of Math. Mech. Vol.76, No.4, 1996, pp 357-360

[12] J. Maas and H. Grotstollen "Simulation Model for Ultrasonic Motors powered by Resonant Converters" . IAS´95, Orlando, Florida,Vol.1, pp. 111-120, Oct. 1995.

[13] J. Maas, T. Schulte and H. Grotstollen "Model-based control of traveling wave type ultrasonic motors ". Proc. of Mechatronics and advanced motion control, Paderborn (Germany), pp. 60-67, may 1999.

[14] J. Maas and H. Grotstollen "Averaged Model of Inverter-Fed Ultrasonic Motors ". PESC´97, Missouri (USA), Vol. 1, pp. 740-786, June 1997.

[15] J. Maas, T. Schulte, and H. Grotstollen, "Optimized drive control for inverter-fed ultrasonic motors," Conf. Rec. IEEE-IAS Annu. Meeting, vol. 1, New Orleans, LA, pp. 690–698, Oct. 1997.

[16] P. Hagedorn, T. Sattel, D. Speziari, J. Schmidt and G. Dianaz " The importance of rotor flexibility in ultrasonic traveling wave motors "Smart Mater. Struc. 7, pp. 352–368, 1998.

[17] Kentaro Nakamura and Sadayuki Ueha "Potential Ability of Ultrasonic Motors: A Discussion Focused on the Friction Control Mechanism" Journal of Electronics and Communications in Japan, Part 2, Vol. 81, No. 4, 1998,pp57-68.

[18] P. LeMoal, P. Cusin "Optimization of traveling wave ultrasonic motors using a three-dimensional analysis of the contact mechanism at the stator–rotor interface" Eur. J. Mech. A/Solids, Vol.18, 1999,pp1061–1084

[19] Nesbitt W Hagood and Andrew J. McFarland "Modeling of a piezoelectric rotary ultrasonic motor", IEEE Trans. Ultrason. Ferroelec. Freq. Contr., Vol.42, No.2, 1995, pp.210-224.

[20] Jürgen Maas, Thomas Schulte, and Norbert Fröhleke "Model-Based Control for Ultrasonic Motors" IEEE Trans. Mechatronics, Vol. 5, No. 2, 2000, pp165-180.

[21] Heiner Storck, and Jörg Wallaschek "The effect of friction reduction in presence of ultrasonic vibrations and its relevance to traveling wave ultrasonic motors" Journal of Ultrasonics, Vol. 40, 2002, pp379-383.

Appendix A : Simulation Parameters of the Shinsei **USR60**

items	Description	*Value*
f	Supply frequency	*41-44khz*
m	Stator mass	*10.1e-3kg*
A_1	Electromechanical coupling of section A	*0.3093*
A_2	Electromechanical coupling of section B	*0.3093*
C_1	Stiffness for sine- mode	*5.97e+8N/m*
C_2	Stiffness for cosine- mode	*5.96e+8N/m*
d_{s1}	Damping for sine- mode	*50Ns/m*
d_{s21}	Damping for cosine - mode	*50Ns/m*
n	Number of nodal diameters	*9*
R_w	Average radius of contact area	*28.75mm*
λ	Wavelength of traveling wave	*20.0713mm*
E	Young's modulus of contact layer	*530N/mm^2*
μ	Coulomb's coefficient of friction	*0.11*
a	Surface distance	*2.5mm*
F_N	Axial applied force	*160N*
m_r	Rotor mass	*30e-3kg*
J	Rotor inertia	*7.2e-6kgm^2*
d_z	Rotor damping	*10e3 Ns/m*
C_z	Rotor stiffness	*300e6 N/m*